

Anisotropic magnetic properties of CeAg₂Ge₂ single crystal

A. Thamizhavel, R. Kulkami and S. K. Dhar

Department of Condensed Matter Physics and Materials Science,

Tata Institute of Fundamental Research, Homi Bhabha Road, Colaba, Mumbai 400 005, India.

(Dated: January 2, 2019)

In order to investigate the anisotropic magnetic properties of CeAg₂Ge₂, we have successfully grown the single crystals, for the first time, by high temperature solution growth (self flux) method. We have performed a detailed study of the grown single crystals by measuring their electrical resistivity, magnetic susceptibility, magnetization, specific heat and magnetoresistance. A clear anisotropy and an antiferromagnetic transition at T_N = 4.6 K have been observed in the magnetic properties. The magnetic entropy reaches R ln 4 at 20 K indicating that the ground state and the first excited state are very closely spaced (a quasi-quartet state). From the specific heat measurements and crystalline electric field (CEF) analysis of the magnetic susceptibility, we have found the level splitting energies as 5 K and 130 K. The magnetization measurements reveal that the a-axis is the easy axis of magnetization and the saturation moment is $s = 1.6 \text{ } \mu\text{B}/\text{Ce}$, corroborating the previous neutron diffraction measurements on a polycrystalline sample.

PACS numbers: 81.10.-h, 71.27.+a, 71.70.Ch, 75.10.Dg, 75.50.Ee

I. INTRODUCTION

In the Ce-based intermetallic compounds, the competition between the RKKY interaction and the Kondo effect leads to diverse ground states. This competition can be readily studied in the multifarious CeT₂X₂ compounds, where T is a transition metal and X is a group IV element namely Si or Ge. CeT₂X₂ compounds crystallize in the well known ThCr₂Si₂ type tetragonal crystal structure and exhibit a wide range of interesting magnetic properties like heavy fermion superconductivity in CeCu₂Si₂¹, pressure induced superconductivity in CePd₂Si₂², CeRh₂Si₂³, unconventional magnetic transition in CeRu₂Si₂⁴ etc. Similarly the isostructural germanides also show interesting magnetic properties^{5,6,7,8}. While most of the above series of silicides and germanides have been grown in single crystalline form and the anisotropic magnetic properties have been investigated, there are no single crystalline reports available on CeAg₂Ge₂ owing to the difficulty in growing the single crystal from a stoichiometric melt. Moreover, the polycrystalline data are also limited. The first report on a polycrystalline CeAg₂Ge₂ was made by Rauchschwalbe et al.⁹ in which they have mentioned that this compound undergoes an antiferromagnetic ordering below 8 K. From neutron scattering experiments an antiferromagnetic ordering temperature of T_N = 7 K was reported by Kopp et al.¹⁰ and Loidl et al.¹¹. Furthermore, an ordered moment of 1.85 $\mu\text{B}/\text{Ce}$ at 1.5 K oriented along the [100] direction was estimated from the neutron scattering experiments. From the specific heat measurements Böhm et al.,¹² have reported that CeAg₂Ge₂ orders antiferromagnetically below 5 K and they observed a peak in the specific heat data at 350 mK when plotted as C = T vs. T (C = C_{nuclear} + C_{magnon}) which they attributed to coherent electronic quasi-particles of medium heavy mass, coexisting with long range magnetic order. However, a recent report by Cordruwisch et al.¹³ have re-

ported a Néel temperature of 4.5 K on a polycrystalline sample. In view of these conflicting reports on the magnetic ordering temperature and to study the magnetic properties more precisely, we have succeeded in growing a single crystal of CeAg₂Ge₂ for the first time and investigated the anisotropic physical properties by means of electrical resistivity, magnetic susceptibility, magnetization, specific heat and magnetoresistance.

II. EXPERIMENT

CeAg₂Ge₂ single crystals were grown by self flux method. Since the use of fourth element as flux normally introduces some inclusions in the grown single crystals, we have grown the single crystals of CeAg₂Ge₂ from an oxygen-stoichiometric melt, with excess of Ag and Ge. The binary phase diagram of Ag and Ge shows an eutectic at 650 °C. We have taken advantage of this eutectic composition and used it as a flux for the growth of CeAg₂Ge₂ single crystal. Similar kind of binary eutectic compositions have been successfully used as flux for the growth of several intermetallic compounds like Au-Si binary eutectic for the crystal growth of CeAu₄Si₂¹⁴, Ag-Ge eutectic flux for the growth of YbAgGe₁₅, Ni-Ge eutectic composition for the growth of several RNi₂Ge₂¹⁶ and Ni-B eutectic composition for the crystal growth of borocarbides¹⁷. The starting materials with 3N-Ce, 5N-Ag and 5N-Ge were taken in the ratio 1 : 16.25 : 6.75 which includes the eutectic composition of the excess flux Ag-Ge. The contents were placed in an alumina crucible, and subsequently sealed in an evacuated quartz ampoule. The temperature of the furnace was raised to 1050 °C and after homogenizing the mixture for two days, the furnace was cooled down to the eutectic temperature of the binary flux Ag-Ge over a period of 3 weeks time and then rapidly to room temperature. The crystals were separated from the flux by means of centrifuging. The

typical size of the crystal was $6 \times 3 \times 0.3$ mm³, with (001) plane as the flat plane.

The dc magnetic susceptibility and the magnetization measurements were performed in the temperature range 1.8–300 K and in magnetic fields up to 7 T along the principal directions using a Quantum Design SQUID magnetometer. The temperature dependence of electrical resistivity in the range 1.8–300 K was measured using a home made DC electrical resistivity set up. The heat capacity and magnetoresistance measurements were performed using a Quantum Design PPM S instrument in the temperature range from 0.5 K to room temperature and for fields up to 12 T.

III. EXPERIMENTAL RESULTS

A. X-ray studies

Since the growth of the single crystals of CeAg₂Ge₂ was performed from an off-stoichiometric starting composition we performed powder X-ray diffraction by crushing a few small pieces of the single crystals to confirm the phase purity of CeAg₂Ge₂. The powder X-ray pattern to-

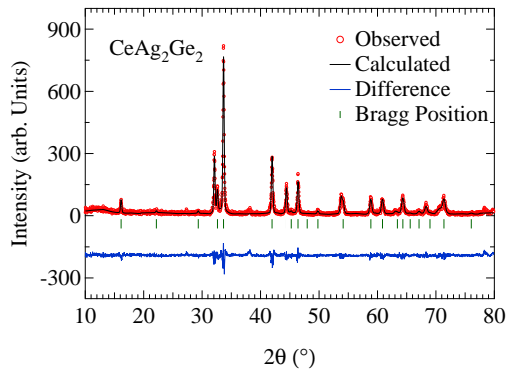


FIG. 1: (Color online) Powder X-ray diffraction pattern recorded for crushed single crystals of CeAg₂Ge₂ at room temperature. The solid line through the experimental data points is the Rietveld refinement profile calculated for the tetragonal CeAg₂Ge₂.

gether with the Rietveld refinement are shown in Fig. 1. The X-ray pattern clearly reveals that the grown single crystals are single phase and no detectable traces of impurity phases are seen. From the Rietveld refinement the ThCr₂Si₂-type crystal structure of CeAg₂Ge₂ is confirmed and the lattice constants were estimated to be $a = 4.301(8)$ Å and $c = 10.973(7)$ Å. We have also performed the energy dispersive X-ray analysis (EDAX) and confirmed the stoichiometry of CeAg₂Ge₂ single crystals. The crystals were then oriented along the principal directions, namely [100] and [001] directions, by means of the Laue back reflection method. Well defined Laue diffraction spots, together with the tetragonal symmetry pat-

tern, indicated the good quality of the single crystals. The crystals were cut along the principal direction using a spark erosion cutting machine for the anisotropic physical property measurements.

B. Electrical resistivity

The dc electrical resistivity of CeAg₂Ge₂ in the temperature range from 1.8 to 300 K is shown in Fig. 2. The

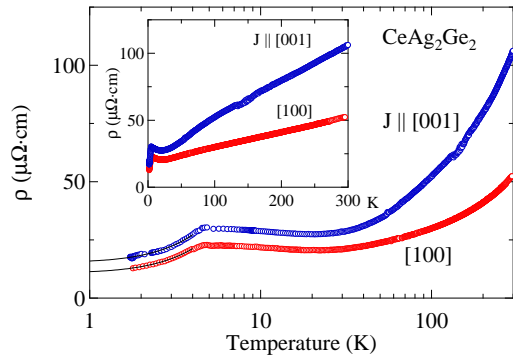


FIG. 2: (Color online) Logarithmic temperature dependence of the dc electrical resistivity of CeAg₂Ge₂ for $J \parallel [100]$ and $[001]$. The inset shows the linear temperature dependence of the electrical resistivity. The solid lines are least square fitting to Eqn. 1.

resistivity was measured for the current direction parallel to [100] and [001]. The electrical resistivity is anisotropic reflecting the tetragonal symmetry of the crystal structure. As it can be seen from the Fig. 2 the absolute value of electrical resistivity at 295 K is 52 $\mu\Omega\text{cm}$ and 106 $\mu\Omega\text{cm}$, respectively for $J \parallel [100]$ and $[001]$ and at 1.8 K is 12 $\mu\Omega\text{cm}$ and 18 $\mu\Omega\text{cm}$ for $J \parallel [100]$ and $[001]$, respectively. At high temperatures the scattering is phonon dominated and the resistivity decreases linearly with decreasing temperature typical of a metallic sample. The electrical resistivity shows a shallow minimum around 20 K and then increases with decrease in temperature up to 4.6 K. This increase in the electrical resistivity at low temperature can be attributed to short range antiferromagnetic order and/or the presence of weak Kondo-type interaction. With further decrease in temperature below 4.6 K, the resistivity changes its slope and drops due to the reduction in spin-disorder scattering caused by the antiferromagnetic ordering of the magnetic moments. Below Néel temperature the electrical resistivity can be explained by a model developed by Continentino et al.¹⁸ which is given by

$$\rho(T) = \rho_0 + A \frac{T^2}{e^{\frac{T}{T_0}}} \left(\frac{1}{1 + \frac{2}{3} \frac{T}{T_N}} + \frac{2}{15} \frac{T^2}{e^{\frac{2T}{T_N}}} \right)^{\frac{1}{2}} \quad (1)$$

This expression is based on scattering of conduction electrons on antiferromagnetic moments with a dispersion relation given by

$$\chi = \frac{P}{\omega^2 + D^2 k^2}; \quad (2)$$

where ω is the spin wave gap and D is the spin wave velocity; $A = 1 = D^3 / \omega^3$ and ϵ is an effective magnetic coupling between Ce ions. A least square fitting of the Eqn. 1 to the experimental electrical resistivity curve of CeAg_2Ge_2 for temperatures less than 4 K results in a very good fit with the parameters $\omega_0 = 10.97$ cm, $A = 0.99$ cm $^{-1}$ K^2 and $\epsilon = 2.73$ K for $H \parallel [100]$ and $\omega_0 = 16.34$ cm, $A = 1.04$ cm $^{-1}$ K^2 and $\epsilon = 4.73$ K for $H \parallel [001]$.

C. Magnetic susceptibility and magnetization

The temperature dependence of magnetic susceptibility in the temperature range from 1.8 to 300 K measured in a field of 1 kOe along the two principal directions viz.,

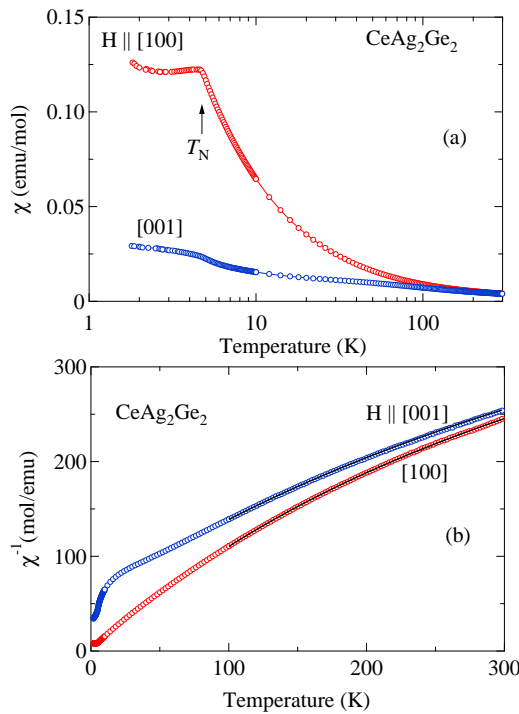


FIG. 3: (Color online) (a) Logarithmic scale of temperature dependence of magnetic susceptibility from 1.8 to 300 K and (b) inverse magnetic susceptibility of CeAg_2Ge_2 . The solid lines in (b) are fitting to the modified Curie-Weiss law.

H parallel to [100] and [001] is shown in Fig. 3(a). Although the anisotropy is small at high temperature, it develops as the temperature is reduced and there is a large anisotropy in the magnetic susceptibility at low temperature. The antiferromagnetic ordering at $T_N = 4.6$ K

is clearly seen as indicated by the arrow. The inverse magnetic susceptibility plot is shown in Fig. 3(b). As it is evident from the Fig. 3(b), the high temperature susceptibility does not obey the simple Curie-Weiss law, on the other hand, it can be very well fitted to a modified Curie-Weiss law which is given by $\chi = \chi_0 + \frac{C}{T - T_p}$, where

χ_0 is the temperature-independent part of the magnetic susceptibility and C is the Curie constant. The main contributions to χ_0 includes the core-electron diamagnetism, and the susceptibility of the conduction electrons. The solid lines in Fig. 3(b) indicate the fitting to the modified Curie-Weiss law with the fitting parameters, $\chi_0 = 1.62 \times 10^{-3}$, $C = 2.42 \mu\text{B}/\text{Ce}$ and $T_p = 1.56$ K for $H \parallel [100]$ and $\chi_0 = 1.50 \times 10^{-3}$, $C = 2.60 \mu\text{B}/\text{Ce}$ and $T_p = -49$ K for $H \parallel [001]$. The average value of the effective magnetic moment amounts to $2.48 \mu\text{B}/\text{Ce}$, which is slightly less than what one would expect for a free Ce^{3+} ion ($2.54 \mu\text{B}/\text{Ce}$). This indicates that the magnetic moments of Ce ions are very well localized in this compound and are essentially in the trivalent state.

The field dependence of isothermal magnetization at $T = 2$ K measured in a SQUID magnetometer up to a field of 70 kOe is shown in Fig. 4. The magnetization

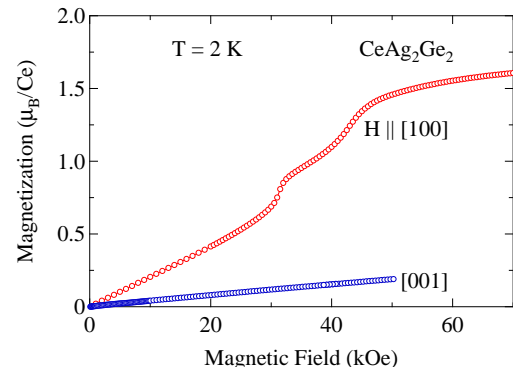


FIG. 4: (Color online) Isothermal magnetization curves of CeAg_2Ge_2 measured at $T = 2$ K along the two principal directions.

curves show large uniaxial magnetocrystalline anisotropy. The magnetization for $H \parallel [100]$ is linear for low fields and shows saturation transitions at critical fields $H_{m1} = 31$ kOe and at $H_{m2} = 44.7$ kOe and nearly saturates at 70 kOe with a saturation magnetization $s = 1.6 \mu\text{B}/\text{Ce}$, this indicates that [100]-axis is the easy axis of magnetization. On the other hand, the magnetization for $H \parallel [001]$ is very small and varies linearly with field reaching a value of $0.32 \mu\text{B}/\text{Ce}$ at 50 kOe, indicating a hard axis of magnetization. We have also performed the isothermal magnetization at 3 K, 4 K, 5 K and 10 K for $H \parallel [100]$ (not shown here). From the differential plots of the isothermal magnetization measurements, we have constructed the magnetic phase diagram as shown in Fig. 5. The two magnetization curves are clearly seen for 2 K and 3 K magnetization curves; however at 3 K only one magnetization transition is seen. For temperatures above the

in magnetic ordering temperature the magnetization curves did not show any metamagnetic behaviour and the magnetization curves were linear indicating a paramagnetic state.

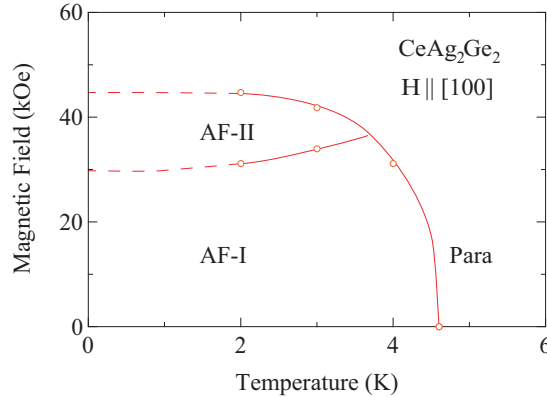


FIG. 5: (Color online) Magnetic phase diagram of CeAg_2Ge_2 for $H \parallel [100]$.

D. Specific heat

Figure 6(a) shows the temperature dependence of the specific heat of a single crystalline CeAg_2Ge_2 together with the specific heat of a polycrystalline reference sample LaAg_2Ge_2 . The low temperature data (1.5 to 10 K) of LaAg_2Ge_2 have been fitted to the expression $C = \gamma T + \beta T^3$ where γ is the electronic contribution and β is the phonon contribution to the heat capacity. The γ and β values thus obtained are estimated to be $2.8 \text{ mJ/K}^2 \text{ mol}$ and $0.59 \text{ mJ/K}^4 \text{ mol}$, respectively. The inset of Fig. 6(a) shows the low temperature part of the specific heat and the antiferromagnetic ordering is manifested by the clear jump in the specific heat at $T_N = 4.6 \text{ K}$ as indicated by the arrow. Figure 6(b) shows the specific heat in the form of $C=T$ versus T . Just below the magnetic ordering the specific heat shows a broad peak in the $C=T$ versus T curve which presumably indicates the presence of low lying crystal field levels. Assuming the lattice heat capacity of CeAg_2Ge_2 is the same as that of LaAg_2Ge_2 , the 4f-derived contribution to the heat capacity C_{mag} was obtained by subtracting the specific heat of LaAg_2Ge_2 from the total specific heat of CeAg_2Ge_2 . Figure 6(c) shows $C_{\text{mag}}=T$ versus T together with the entropy S_{mag} which is obtained by integrating $C_{\text{mag}}=T$. As it can be seen from the figure, the entropy of CeAg_2Ge_2 is very high at the magnetic ordering temperature and reaches $R \ln 4$ near 20 K. In tetragonal symmetry, the degenerate six fold levels of the ground-state multiplet of Ce^{3+} split into three doublets and 1_1 and 1_2 are the excitation energies of the first and second excited states, respectively. Since the entropy change reaches $R \ln 4$, not too far above T_N , one can come to a conclusion that the ground state and the first excited state are very closely

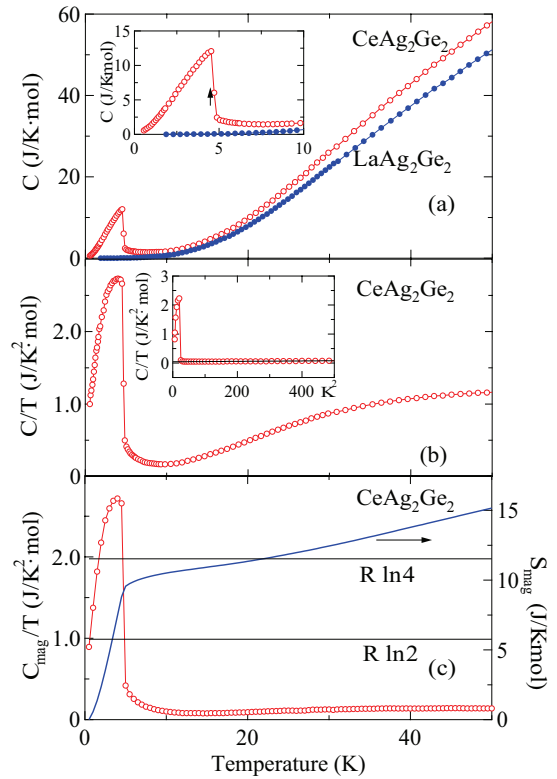


FIG. 6: (Color online) (a) Temperature dependence of the specific heat of CeAg_2Ge_2 and LaAg_2Ge_2 , and (b) specific heat of CeAg_2Ge_2 in the form of $C=T$ versus T . (c) magnetic specific heat C_{mag} in the form of $C_{\text{mag}}=T$ versus T together with the magnetic entropy S_{mag} .

spaced or nearly degenerate. This finding clearly corroborates the earlier neutron diffraction results by Loidl et al.¹¹ in which they could observe only one crystal field transition at 11 meV and concluded that the ground state is almost degenerate with the first excited state.

From the crystalline electric field analysis of the magnetic susceptibility data, to be discussed later, we found that the energies of the excited states 1_1 and 1_2 as 5 K and 130 K, respectively. Due to the very small splitting energy between the ground state and the first excited state the estimation of the Sommerfeld coefficient, by the usual method, from the low temperature data will lead to ambiguity. Hence we estimated the value from the high temperature data in the paramagnetic region above the magnetic ordering after subtracting the Schottky contribution and linearly extrapolating the $C=T$ versus T^2 behaviour to $T = 0 \text{ K}$ and is shown in the inset of Fig. 6(b). The value thus estimated is $45 \text{ mJ/K}^2 \text{ mol}$.

E. Magnetoresistance

We have also studied the effect of magnetic field on the resistivity of CeAg_2Ge_2 . The magnetic field did not have any appreciable effect on the resistivity for the field

perpendicular to the easy axis direction. On the other hand, when the field was applied parallel to the easy axis direction, we found that the resistivity gradually decreased with increasing field. In Fig. 7 we have plotted

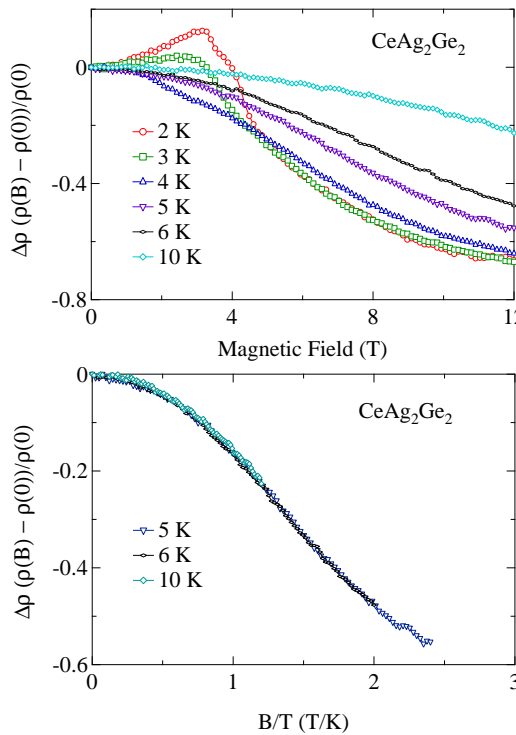


FIG. 7: (Color online) (a) Isothermal normalized magnetoresistance for CeAg₂Ge₂ as function of applied magnetic field for J_k [100] and H_k [100]. (b) Normalized magnetoresistivity plotted as a function of $B=T$.

the normalized magnetoresistance $\Delta\rho = \rho(B) - \rho(0) = [(\rho(B) - \rho(0))/\rho(0)]/[(B - 0)/B_0]$ as a function of applied magnetic field at various fixed temperatures. With increasing magnetic field for H_k [100], $\Delta\rho$ at 2 K initially increases in the positive direction and then turns negative at higher magnetic fields, giving rise to a maximum at 3.1 T. This field value coincides with the metamagnetic transition observed in the magnetization measurement at $T = 2$ K. Such a behaviour of the magnetoresistance is qualitatively consistent with the theoretical calculation given by Yamada and Takada¹⁹. In the antiferromagnetic state ($H < H_m$), the magnetism moment fluctuation in one magnetic sublattice is enhanced by the field while, in the field induced ferromagnetic state ($H > H_m$), the fluctuation is suppressed by the field. The change in the fluctuation is reflected in the magnetoresistance. With the increase in the temperature, the peak in the magnetoresistance moves toward lower fields and decreases, finally disappears for temperatures above T_N . In the paramagnetic region the negative magnetoresistance is due to the freezing out of the spin- $\frac{1}{2}$ scattering by the magnetic field. The normalized magnetoresistance for $T > T_N$ can be mapped onto a single curve as shown in Fig. 7(b) when

plotted as a function of $B=T$. In Kondo compounds, the normalized magnetoresistance obeys the scaling law $B=(T+T_0)$ where T_0 is the characteristic temperature which is an approximate measure of the Kondo temperature T_K ²⁰. Since in CeAg₂Ge₂ the magnetoresistance scales as a function of $B=T$, we can say that T_K must be very low in this compound.

IV. DISCUSSION

From the results of the electrical resistivity, susceptibility and specific heat measurements it can be clearly seen that CeAg₂Ge₂ undergoes an antiferromagnetic ordering at 4.6 K with the easy axis of magnetization as [100]. The magnetization at 70 kOe reaches 1.6 μ_B/C_e thus corroborating the earlier neutron scattering experiment¹¹ on a polycrystalline sample of CeAg₂Ge₂. The electrical resistivity at high temperature shows a typical metallic behaviour and at sufficiently low temperature it shows a weak minimum before ordering magnetically. This behaviour is quite different from what one has observed in the CeCu₂Ge₂ which is similar to CeAg₂Ge₂ both structurally and magnetically, although the antiferromagnetic ordering temperature is nearly equal ($T_N = 4.1$ K for CeCu₂Ge₂ and $T_N = 4.6$ K for CeAg₂Ge₂). The logarithmic temperature dependence of electrical resistivity in CeCu₂Ge₂ exhibit a double peak structure which is presumably attributed to the combined influence of the Kondo and crystalline electric field (CEF) effects. The Kondo temperature of CeCu₂Ge₂ was estimated to be about 6 K²¹, whereas for CeAg₂Ge₂ the Kondo temperature is very small. Since the unit cell volume of CeCu₂Ge₂ is smaller ($V = 178 \text{ \AA}^3$), a larger value of the Kondo coupling constant J_{sf} is expected and hence the Kondo interaction dominates in CeCu₂Ge₂ compared to that in CeAg₂Ge₂ ($V = 203 \text{ \AA}^3$). In CeCu₂Ge₂ superconductivity occurs when the unit cell volume attains a favourable value of $168 \text{--} 3 \text{ \AA}^3$. This is achieved with an external pressure of 7 GPa. Considering this fact the unit cell volume of CeAg₂Ge₂ is quite large and one would require a very high pressure to reduce the unit cell volume to nearly $168 \text{--} 3 \text{ \AA}^3$ for probable observation of superconductivity. Based on this it can be said that CeAg₂Ge₂ lies on the left hand side of the Doniach phase diagram in which the RKKY energy scale is dominant and Kondo interaction is weak.

The heat capacity measurement of CeAg₂Ge₂ single crystal clearly reveals the presence of low lying crystal field levels with a very small separation between the ground state and the first excited state indicating that the ground state is a quasi-quartet state instead of a doublet which is usually observed for a tetragonal site symmetry. In order to further analyze the crystal field levels and to understand the present anisotropy in the magnetic susceptibility we have performed the CEF analysis on the susceptibility data. For the purpose of CEF analysis in Fig. 8 we have plotted the experimental results

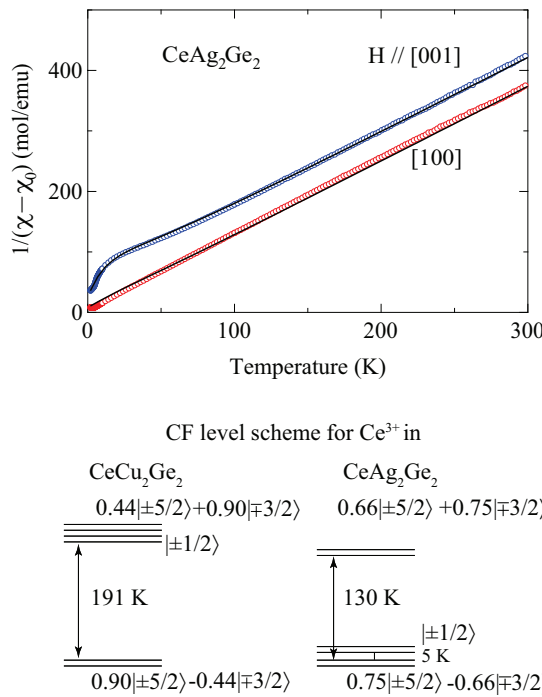


FIG. 8: (Color online) Temperature dependence of the inverse magnetic susceptibility in CeAg_2Ge_2 . Solid lines are fitting to the CEF level scheme with a molecular field term. The bottom figure shows the crystal-field level scheme of Ce^{3+} in the CeCu_2Ge_2 (taken from Ref.21) and CeAg_2Ge_2 .

on susceptibility in the form of $1 = (1 - \chi_0)$, where χ_0 was determined as 1.33×10^{-3} and 1.41×10^{-3} emu/mol for $H \parallel [001]$ and $[100]$, respectively, so an effective magnetic moment of $2.54 \mu_B/\text{Ce}$ is obtained above 100 K. Similar kind of treatment has been made for CePt_3S_2 while performing the CEF analysis. The Ce atoms in CeAg_2Ge_2 possess the tetragonal site symmetry and hence the CEF hamiltonian is given by,

$$H_{\text{CEF}} = B_2^0 O_2^0 + B_4^0 O_4^0 + B_4^4 O_4^4; \quad (3)$$

where B^m and O^m are the CEF parameters and the Stevens operators, respectively^{23,24}. The magnetic susceptibility including the molecular field contribution is given by

$$\chi = \frac{1}{C_{\text{EF}}} \quad ; \quad (4)$$

where C_{EF} is the CEF susceptibility. Diagonalization of the CEF Hamiltonian gives us the eigenvalues

and eigenfunctions. For Ce^{3+} $J = 5/2$ wave function splits into three doublets, ${}_7^{(1)} = a j 5/2i + b j 3/2i$, ${}_7^{(2)} = a j 3/2i - b j 5/2i$ and ${}_6 = j 1/2i$, where a and b are mixing parameters with the condition $a^2 + b^2 = 1$. The CEF parameters were estimated from the fits to the magnetic susceptibility. Solid lines in Fig. 8 show the least square fitting to Eqn. 4, the CEF parameters thus obtained are listed in Table I. The corresponding crystal field level scheme together with that of CeCu_2Ge_2 is shown in the bottom part of Fig. 8. The crystal field level scheme for CeCu_2Ge_2 is taken from Ref.21. The ground state of CeAg_2Ge_2 shows a mixing of $j 3/2i$ and $j 5/2i$ wave functions. From Fig. 8 it is obvious that the present set of CEF parameters gives a good fit to the experimental data thereby explaining the anisotropy in the magnetic susceptibility. The CEF parameters have resulted in the first and second excited states at $T_1 = 5$ K and $T_2 = 130$ K. It is interesting to note here that the CEF level scheme of CeCu_2Ge_2 is qualitatively opposite to the present case where the ground state is a doublet and the first and second excited states are nearly degenerate. This can be explained on the basis of the sign of the B_2^0 parameter. For CeCu_2Ge_2 it is negative while it is positive for CeAg_2Ge_2 . This change in sign of B_2^0 suggests that the CEF potential in CeT_2Ge_2 is largely dependent on the hybridization between localized f-electron states and the conduction-electron bands.

V. CONCLUSION

Single crystals of CeAg_2Ge_2 have been grown for the first time, by flux method by using a Ag-Ge binary eutectic composition as flux. The antiferromagnetic ordering temperature $T_N = 4.6$ K is clearly manifested by the resistivity, heat capacity and susceptibility measurements. Thus the ambiguity about the magnetic ordering temperature of this compound, reported in the conflicting reports earlier in the literature, has been removed. A large anisotropy in the electrical resistivity, magnetic susceptibility and magnetization is observed. The susceptibility and magnetization clearly reveals that $[100]$ -axis as the easy axis of magnetization with a moment of $1.6 \mu_B/\text{Ce}$ at 70 kOe. Magnetization transitions have been observed at the critical fields, $H_{m1} = 31$ kOe and at $H_{m2} = 44.7$ kOe. The heat capacity and the susceptibility data clearly support the closely spaced ground and first excited states, which have been analyzed by the CEF calculations.

¹ F. Steglich, J. Aarts, C. D. Bredl, W. Lieke, D. M. Eschede, W. Fraz and H. Schafer, Phys. Rev. Lett. 43, 1892 (1979).

² I. Sheikin, E. Steep, D. Braithwaite, J.-P. Brison, S. Raymond, D. Jaccard and J. Flouquet, J. Low Temp. Phys. 122, 591 (2001).

³ R. M. Ovshovitch, T. G. RAF, D. M. Andrus, J. D. Thompson, J. L. Smith and Z. Fisk, Phys. Rev. B 53, 8241 (1996).

⁴ P. Haen, J. Flouquet, F. Labeyrie, P. Lejay and G. Remenyi, J. Low Temp. Phys. 67, (1987) 391.

⁵ H. Abe, K. Yoshii and H. K. Itazawa, Physica B 312-313,

TABLE I: CEF parameters, energy level schemes and the corresponding wave functions for CeAg₂Ge₂.

CEF parameters		B ₂ ⁰ (K)	B ₄ ⁰ (K)	B ₄ ⁴ (K)	i (emu/mol)	¹
		2.24	0.19	2.40	[100] =	7.2
energy levels and wave functions						
E (K)	j+5=2i	j+3=2i	j+1=2i	j=1=2i	j=3=2i	j=5=2i
130	0.656	0	0	0	0.754	0
130	0	0.754	0	0	0	0.656
5	0	0	0	1	0	0
5	0	0	1	0	0	0
0	0	0.656	0	0	0	0.754
0	0.754	0	0	0	0.6565	0

253 (2002).

⁶ S. Rayment, P. H. Aen, R. Calemzuk, S. Kamle, B. Fak, P. Lepy, T. Fukuhara and J. Flouquet, *J. Phys.: Condens. Matter* 11, 5547 (1999).

⁷ T. Fukuhara, K. Maezawa, H. Ohkuni, J. Sakurai and H. Sato, *J. Magn. Magn. Mater.* 140-144, 889 (1995).

⁸ F. M. G. rosche, P. A. Garwal, S. R. Julian, N. J. Wilson, R. K. W. Haselwimmer, S. J. S. Lister, N. D. M. Athur, F. V. Carter, S. S. Saxena and G. G. Lonzarich, *J. Phys.: Condens. Matter* 12, L533 (2000).

⁹ R. Rauchschwalbe, U. G. ottwick, U. Ahlheim, H. M. M. ayer and F. Steglich, *J. Less Common. Metals* 111, 265 (1985).

¹⁰ G. Knopp, H. Spille, A. Loidl, K. Knorr, U. Rauchschwalbe, R. Felten, G. Weber, F. Steglich and A. P. M. urani, *J. Magn. Magn. Mater.* 63 & 64, 88 (1987).

¹¹ A. Loidl, K. Knorr, G. Knopp, A. Krimmel, R. Caspary, A. Bohm, G. Spahn, C. Geibel, F. Steglich and A. P. M. urani, *Phys. Rev. B* 46, 9341 (1992).

¹² A. Bohm, R. Caspary, U. Habel, L. Pawlak, A. Zuber F. Steglich and A. Loidl, *J. Magn. Magn. Mater.* 76 & 77, 150 (1988).

¹³ E. C. Ordruish, D. Kaczorowski, A. Saccone, P. Rogl and R. Ferro, *J. Phase Equilibria* 20, 407 (1999).

¹⁴ H. Nakashima, A. Thamizhavel, T. D. Matsuura, Y. Haga, T. Takeuchi, K. Sugiyama, R. Settai and Y. Onuki, *J. Alloys Compd.* 424, 7 (2006).

¹⁵ E. M. Orosan, S. L. Bud'ko, P. C. Canfield, M. S. Torikachvili and A. H. Lacerda, *J. Magn. Magn. Mater.* 227, 298 (2004).

¹⁶ S. L. Bud'ko, Z. Islam, T. A. Wiener, I. R. Fisher, A. H. Lacerda, P. C. Canfield, *J. Magn. Magn. Mater.* 205, 53 (1999).

¹⁷ P. C. Canfield, I. R. Fisher, *J. Crystal Growth* 225, 155 (2001).

¹⁸ M. A. Continentino, S. N. de Medeiros, M. T. D. Orlando, M. B. Fontes and E. M. Baggio-Saitovitch, *Phys. Rev. B* 64, 012404 (2001).

¹⁹ H. Yamada and S. Takada, *Prog. Theor. Phys.* 49, 1401 (1973).

²⁰ P. Schlottmann, *Z. Phys. B: Condens. Matter* 51, 223 (1983).

²¹ G. Knopp, A. Loidl, K. Knorr, L. Pawlak, M. Duczmal, R. Caspary, U. G. ottwick, H. Spille, F. Steglich and A. P. M. urani, *Z. Phys. B - Condensed Matter* 77, 95 (1989).

²² T. Takeuchi, S. Hashimoto, T. Yasuda, H. Shishido, T. Ueda, M. Yamada, Y. Obizaki, M. Shiimoto, H. Kohara, T. Yamamoto, K. Sugiyama, K. Kondo, T. D. Matsuura, Y. Haga, Y. Aoki, H. Sato, R. Settai and Y. Onuki, *J. Phys.: Condens. Matter* 16, L333 (2004).

²³ K. W. H. Stevens, *Proc. Phys. Soc., London, Sect. A* 65, 209 (1952).

²⁴ M. T. Hutchings, in *Solid State Physics: Advances in Research and Applications*, edited by F. Seitz and B. Turnbull (Academic, New York, 1965), Vol. 16, p. 227.